Computerized Medical Imaging and Graphics 37 (2013) 150–161

Contents lists available at SciVerse ScienceDirect

Computerized Medical Imaging and Graphics

journal homepage: www.elsevier.com/locate/compmedimag

Automatic and efficient contrast-based 2-D/3-D fusion for trans-catheter aortic valve implantation (TAVI)

Rui Liao*, Shun Miao, Yefeng Zheng

Imaging and Computer Vision, Siemens Corporation, Corporate Technology, Princeton, NJ, USA

ARTICLE INFO

Article history:
Received 28 March 2012
Received in revised form
21 December 2012
Accepted 23 January 2013

Keywords:
Image-guided intervention
2-D/3-D registration
Contrast agent inflow detection
Minimally invasive procedures
Trans-catheter aortic valve implantation

ABSTRACT

Trans-catheter aortic valve implantation (TAVI) is a new breakthrough in the field of minimally invasive surgery applied on high-risk patients with aortic valve defects. 2-D X-ray angiographic and fluoroscopic images are typically used to guide TAVI procedures, for which contrast agent needs to be injected from time to time in order to make the anatomy of the aortic root visible under X-ray. Advanced visualization and guidance technology involving patient-specific 3-D models of the aorta can greatly facilitate the relatively complex TAVI procedures by providing a more realistic anatomy of the aortic root and more accurate C-Arm angulation. In this paper, a fully automatic and efficient system for contrast-based 2-D/3-D fusion for TAVI is presented. Contrast agent injection into the aortic root is automatically detected based on histogram analysis and a likelihood ratio test on the X-ray images. A hybrid method is then applied for contrast-based 2-D/3-D registration between the 3-D model and the detected angiographic frame. By integrating the information of aorta segmentation and aortic landmark detection into intensity-based registration, the proposed method combines the merits of intensity-based registration and feature/landmark-based registration. Experiments on 34 clinical data sets from TAVI patients achieve 100% correct detection on the contrast-enhanced frame, and a mean registration error of 0.66 ± 0.47 mm for 2-D/3-D registration. The proposed method is furthermore highly efficient with an average processing time of 2.5 s after the most contrast-enhanced frame is available, demonstrating the efficacy of the proposed method to be adopted in a clinical setup.

1. Introduction

Aortic valve disease is affecting 1.8% of the global population and is the most frequent heart valve disease in developed countries. There are about 60,000 surgical aortic valve replacements every year in Europe and even more in the United States [1]. Although open heart surgery is a well-established procedure with a proven success rate, one-third of TAVI candidates are denied surgery, particularly in the elderly, because of a perceived high operative risk. Compared to traditional open surgery, trans-catheter approaches deliver the prosthetic valve via a small incision at the patient's chest or groin. It is best-suited for high-risk patients with severe aortic stenosis, and has the potential to be applied to regular-risk patients in the future. TAVI has already accounted for more than 20% of aortic valve replacement procedures in Germany. It is also expected to grow fast in the United States in the coming 2–3 years after the recent FDA approval for commercial use of the Edwards SAPIEN valve [2]. Furthermore, the recent randomized trials show that TAVI significantly reduces the mortality rate for patients who are denied surgery, compared to the current standard medical therapy, and has a comparable outcome to open heart surgery for high-risk patients who can undergo surgery [3].

During TAVI procedures, X-ray angiographic and fluoroscopic imaging is routinely used to guide the operation, because the visibility of the target area is limited to the naked eyes due to the small incisions. However, fluoroscopic images do not display the anatomic structures without the contrast agent, which on the other hand needs to be minimized for patients' safety. Recently, 3-D models were introduced to support TAVI procedures by overlaying the 3-D aortic model onto fluoroscopy. Introduction of the patient-specific 3-D model of the aortic root has the advantages of displaying more realistic anatomical details and providing more automatic and accurate C-Arm angulation for optimal valve deployment [4]. The 3-D aortic model can be derived from pre-operative high-resolution computed tomography (CT) and magnetic resonance imaging (MRI) volumes, or from an intra-operative C-Arm CT volume [5].

In this paper, a fully automatic and highly efficient system for 2-D/3-D fusion of the 3-D model and angiography/fluoroscopy during TAVI procedures is presented. The whole system consists

* Corresponding author. Tel.: +1 609 734 3375; fax: +1 609 734 6565.
E-mail address: rui.liao@siemens.com (R. Liao).

0895-6111/$ – see front matter © 2013 Elsevier Ltd. All rights reserved.
http://dx.doi.org/10.1016/j.compmedimag.2013.01.008

of C-Arm CT acquisition and reconstruction, automatic 3-D aorta segmentation and landmark detection on the C-Arm CT volume, optimized volume visualization and derivation of the optimum C-Arm angulation, and 2-D/3-D fusion for navigation and guidance. The focus of this paper is automatic contrast-based 2-D/3-D registration between the 3-D model and 2-D angiography, to compensate for motions such as patient movement and aortic root movement due to the insertion of the devices. Contrast agent injection into the aortic root is automatically detected on X-ray images based on the method presented in [6,7], and the positive response to contrast agent inflow detection is then used to automatically trigger 2-D/3-D registration between the 3-D model and the angiography showing the aortic root [8]. A seamless workflow and accurate registration between the pre-operative 3-D model and the patient undergoing the procedure are the key components for a successful image guidance system for TAVI, which is a relatively complicated procedure involving a large number of staff, equipment and steps [2–5].

Techniques for 2-D/3-D registration between 3-D volumes and 2-D X-ray images can be divided into two general groups: landmark/feature-based methods and intensity-based methods. Landmark/feature-based methods [9–11] register landmarks and/or salient features that have been extracted automatically or semi-manually from both the 2-D image and the 3-D volume. While this approach exhibits fast execution time and high robustness in the face of large initial misalignment, it is difficult to achieve full automation, especially for salient feature extraction from 2-D X-ray images that inherently suffer from overlapping and/or foreshortening due to 2-D projections. For intensity-based registration algorithms [12–14], simulated X-ray images are produced from the 3-D volume, and are referred to as digitally reconstructed radiographs (DRRs). The translation and rotation of the 3-D volume are estimated through an optimal match between the DRRs and the X-ray image. While intensity-based methods have been shown to give substantially more reliable results than their feature-based counterparts, its accuracy may be sub-optimal at the structure of interest, and its performance is seriously deteriorated when there is mismatch between the contents shown in the 2-D and 3-D data.

This paper describes a hybrid method that incorporates the segmentation and landmark information of the 3-D aortic root into intensity-based registration, for a highly accurate and robust 2-D/3-D alignment of the aorta. Both the 3-D volume and the 2-D images are captured with contrast agent showing the patient's aortic root. 2-D angiographic images are first pre-processed to remove the background and/or devices such as the catheter and TEE probe. 3-D aorta segmentation and coronary ostia landmark detection is performed on the 3-D volume using the learning-based method presented in [5]. The segmented aorta and detected landmarks are given inputs to our algorithm. Discussion on the accuracy of the segmentation step is out of the scope of this paper, and readers are referred to [5] for more details. Aorta segmentation is then used to produce clean DRR images that show only the aorta and excludes all the peripheral structures such as the spine. Landmarks representing the left and right coronary ostia are further utilized in an integrated fashion with the intensity-based method. A multi-layer and multi-resolution optimization strategy is finally deployed to find the optimal registration.

The remainder of the paper is organized as follows. A brief overview of the image-guided system for 2-D/3-D fusion during TAVI is given in Section 2. Methods for efficient and accurate contrast-based 2-D/3-D registration between the 3-D model and the angiography are covered in Section 3. Experiments are performed on a large number of clinical datasets and the quantitative results are reported in Section 4. We then conclude with Section 5 for discussion and future work.

2. Overview of image-guided system for TAVI

Previous work on computer-based support for TAVI includes the modeling for procedure planning [15,16], guidance by tracking the prosthetic valve in fluoroscopic images [17], a robotic system using MRI imaging [18], and fusion between ultrasound and fluoroscopic images [19]. The goal of our fusion system is to provide image guidance based on interventional C-Arm CT volumes to add detailed 3-D information that is helpful for an accurate navigation and deployment of the prosthetic valve. The system needs to be set up in the complex environment of a hybrid operating room and used by a physician during TAVI procedures without additional support from the control room. Therefore, it is crucial for the acceptance of such a system to be fast, to minimize user interactions, and to allow table-side control. We give a brief overview of the proposed system here, though a more detailed description of our prototype system that is currently under clinical trial can be found in [4].

Right before placing the implant, an interventional 3-D C-Arm CT volume of the aortic root is obtained by acquiring a rotational 2-D image sequence of 200° over 5 s on the C-Arm system [20]. The rotational run is then reconstructed based on a software available with the C-Arm system [21], which takes about 12 s. The aortic root is then segmented and eight landmarks are detected from the reconstructed C-Arm CT volume using the method in [5]. This step is automatically triggered after a valid aortic C-Arm CT volume is reconstructed, and is fully automated and very efficient, taking about 2.5 s on average. The eight landmarks include the lowest point of each aortic root cusp (hinge points), the coronary artery ostia, and the commissure points where the cusps meet. Additional structures/measurements and subsequently the optimum C-Arm angulations are then automatically derived from the segmentation of the aorta and the detected landmarks. In particular, we derive a circle parallel to the plane spanned by the three hinge points, and an optimal C-Arm angulation for valve implantation is achieved when this circle degenerates to a straight line (Fig. 1). Optimized visualization of the aortic root is further automated as outlined next, which takes less than 1 s on average. The last step of the image guidance system is 2-D/3-D overlay of the 3-D model onto the fluoroscopic/angiographic live images for online monitoring and navigation. A flowchart for all the steps supported intra-operatively using our prototype system is given in Fig. 2.

Volume rendering of the 3-D model is optimized using a learning based method, which learns the optimal rendering parameters from training examples that are manually adjusted by an expert for an optimized visualization. In particular, the appropriate volume rendering parameters c_{opt} for the transfer function center and w_{opt} for the transfer function width are calculated automatically based on the voxel intensities:

$$\begin{aligned} c_{opt} &= f_{c,in} m_{in} + f_{c,out} m_{out} + f_{c,offset} \\ w_{opt} &= f_{w,in} m_{in} + f_{w,out} m_{out} + f_{w,offset} \end{aligned} \tag{1}$$

Here, m_{out} (m_{in}) is a patient-specific value and is determined by the mean intensities of all the voxels outside (inside) the boundary of the segmented aortic root with a fixed distance to it. The underlying set of voxels is computed using the morphologic operators of dilation and erosion with a certain number of iterations. The six parameters $f_{c,in}, f_{c,out}, f_{c,offset}, f_{w,in}, f_{w,out}, f_{w,offset}$ in Eq. (1) are fixed values that are obtained by a training sample set of segmented volumes. For each of these training volumes we manually adjust optimal window width and window center values. Together with the calculation of the corresponding values m_{in} and m_{out} we get an over-determined system of linear equations with six unknown parameters, which are then solved by a least-square fitting method.

When overlaying the 3-D model onto a live fluoroscopic image, we offer the options of volume, mesh, and contour view of the

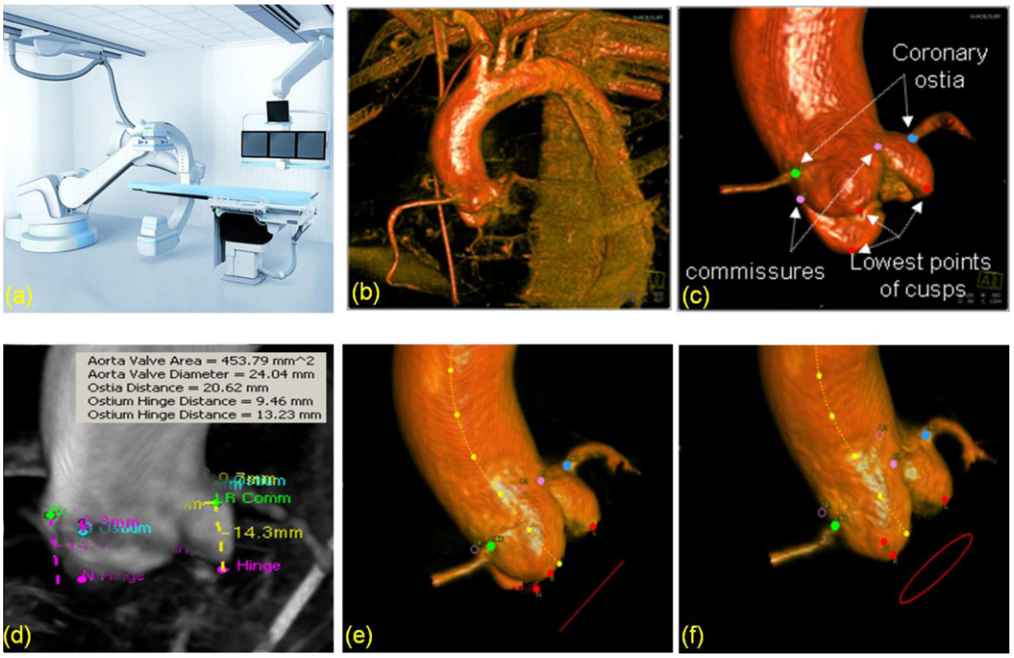

Fig. 1. Trans-catheter aortic valve implantation under X-ray guidance. (a) Angiographic C-Arm system to acquire interventional 3-D C-Arm CT volumes in an operating room; (b) the reconstructed C-Arm CT volume; (c) aorta segmentation and landmark detection; (d) measurements derived from segmentation and landmarks; (e) an optimal C-Arm angulation where the circle parallel to the hinge plane degenerates to a line; and (f) an non-optimal C-Arm angulation.

aortic root (Fig. 3). The contour view yields the best fluoroscopic image quality in the overlay by showing only the essential information needed for prosthesis positioning and deployment, and hence is often the preferred choice. The contours are computed by an efficient edge detection method. Firstly, a volume rendered aortic root image is segmented by simple image intensity thresholding. Secondly, gradients of the segmented pixels are calculated. The maximum gradient value is also assigned to border pixels (pixels with at least one neighboring background pixel). Thirdly, edge pixels are detected by hysteresis thresholding (similar to the Canny edge detector) on the gradient values. Finally, connected components with a small number of detected edge pixels are removed.

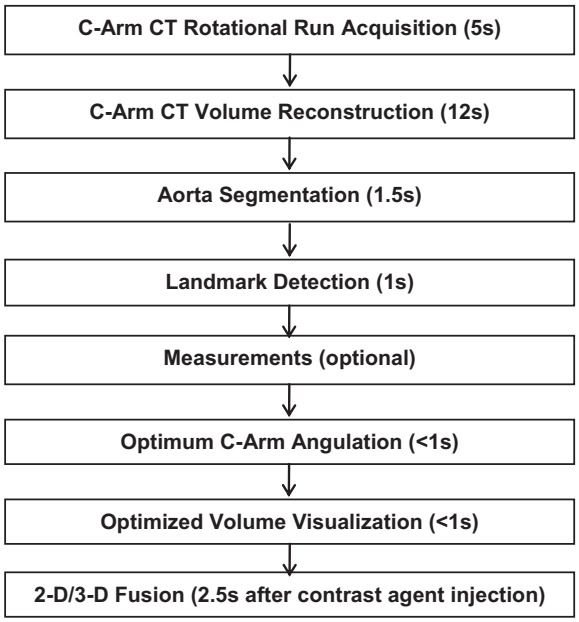

Fig. 2. A flowchart for all the steps supported intra-operatively by our image guidance system and the typical time needed for each step.

The 2-D/3-D fusion prototype is currently under clinical trial and has been installed in more than 10 hospitals around the world. The system is very fast and the workflow is optimized for minimal user interaction, i.e. the only possible user interaction is when the physician wants to manually edit the position of the detected landmarks. In practice, landmark adjustments are only rarely done by the user. The parameters of window-levels for volume visualization are obtained offline using 110 training volumes from 3 different hospitals, and the automatically optimized volume and contour visualization provides clinically satisfactory results in our clinical trial so far. A few examples are shown in Fig. 4. Up to date our clinical prototype has been used in assisting more than 1000 TAVI cases and in all the cases done so far the system runs stably with a seamless workflow.

3. Efficient contrast-based 2-D/3-D registration

Since the 3-D C-Arm CT volume and 2-D fluoroscopic/angiographic images are acquired on the same machine, they can be registered based on machine calibration when there is no patient movement. However, clinically it is often observed that there is significant relative motion between the two image data sets as a result of aorta deformation introduced by, for example, the insertion of the pigtail catheter and the prosthetic valve, heart shift due to rapid pacing deployed during the acquisition of the 3-D volume to minimize motion blurring, and patient gross movement. Motion compensation hence is indispensable for an accurate 2-D/3-D fusion in our TAVI image guidance system. We propose to tackle this motion compensation problem by first automatically detecting the X-ray frame showing adequate contrast agent in the aortic root and then performing efficient contrast-based 2-D/3-D registration between the 3-D model and the detected contrast-enhanced frame.

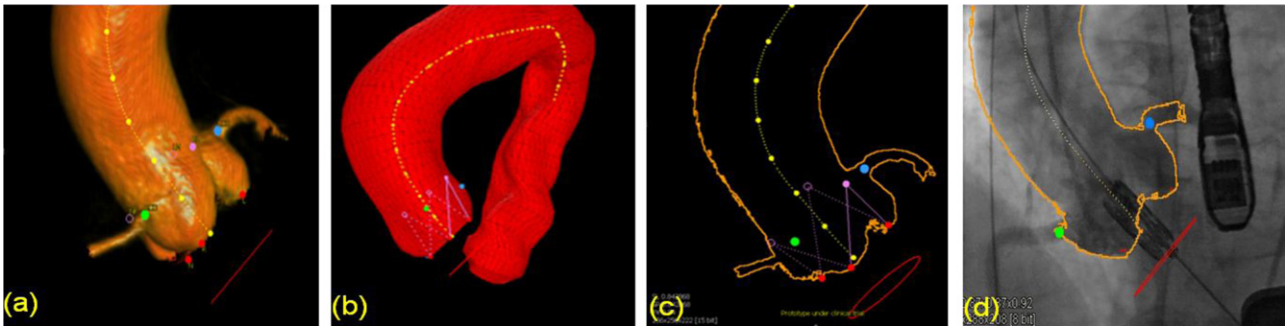

Fig. 3. Aortic root visualization. (a) Volume rendering, (b) mesh visualization, (c) contour visualization, and (d) overlay of the contour onto an angiography.

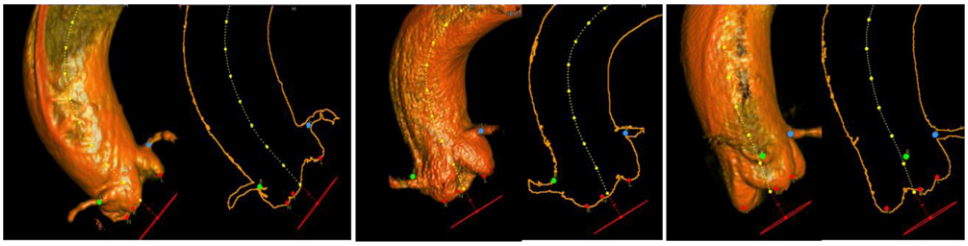

Fig. 4. Examples of the automatically optimized volume and contour visualization.

3.1. Automatic detection of the contrast-enhanced frame

Only a few research publications address the problem of automatic detection of contrast medium injection on a fluoroscopic/angiographic sequence. The method in [22] uses simple hard-coded thresholds on the histogram percentile and hence is difficult to handle the drastic variations in our TAVI data acquired from different clinical sites using different protocols and on different patients. Recently, a learning-based method was proposed in [23] to detect contrast medium injection into the coronary artery. The method focuses on the vessel structures, and hence cannot be directly applied for our application because the variations at the contrast-enhanced aortic root are much more profound than that at the coronary artery ostia due to the extremely fast wash-out of the contrast medium from the aorta. Furthermore, there will be no such a dominant feature as the "vesselness" in [23] to be used as the base feature for training for our application.

In [6,7] we proposed a novel integrated spatial and temporal analysis for automatic detection of contrast agent injection into the aortic root on fluoroscopic and angiographic sequences. The proposed method is based on histogram analysis and a likelihood ratio test. In particular, for each frame in the sequence, we introduce a contrast feature value as the ratio of its histogram similarities to the reference histograms with and without contrast agent presence, respectively. This contrast feature value has many robust properties, for example, insensitive to the change of the absolute value in image intensity, the size of the aorta, and the volume and density of the injected contrast medium. A temporal curve, denoted as contrast feature curve, plots the contrast feature value versus frame index. In general, a contrast feature curve contains a dominant

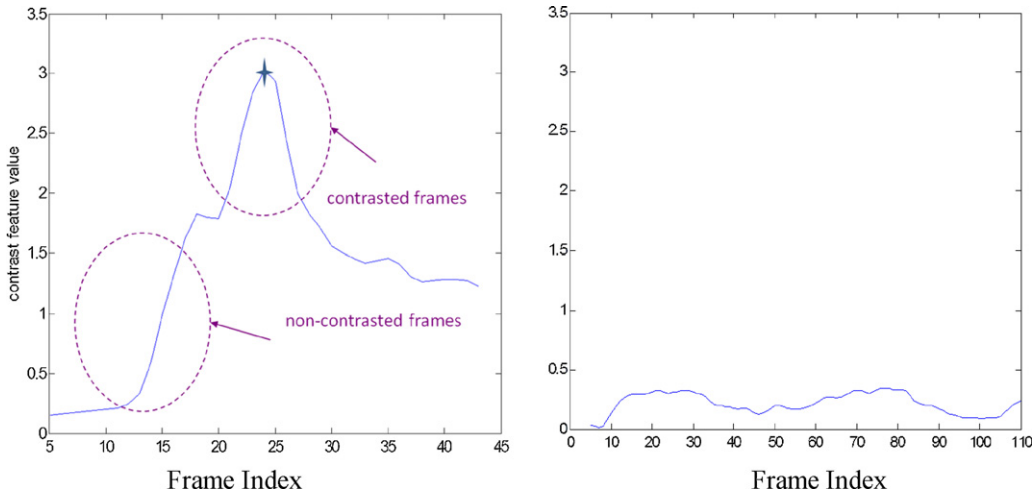

Fig. 5. Left: the contrast feature curve for a sequence with contrast agent injection, with the detected peak marked by a star. Right: the contrast feature curve for a sequence without contrast agent injection.

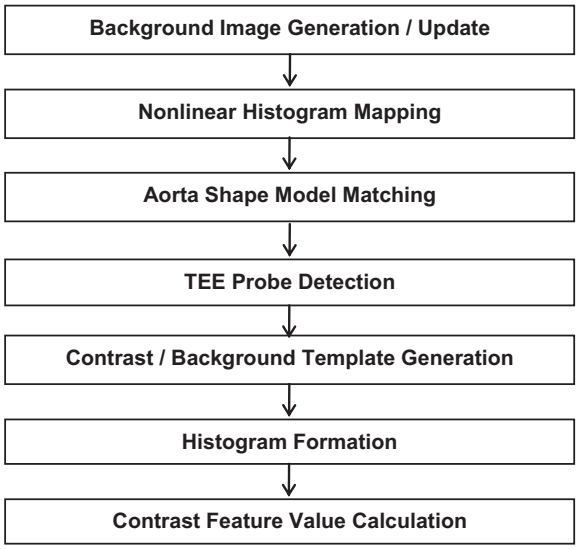

Fig. 6. Workflow diagram for contrast feature value calculation.

peak for a sequence with contrast agent, and is relatively flat for a sequence without contrast medium (Fig. 5). These desired properties make the contrast feature curve a great candidate to identify frames with contrast agent presence in a fluoroscopic and/or angiographic sequence.

A diagram of the algorithm workflow for calculating the contrast feature value is shown in Fig. 6: (1) a background image is calculated by averaging several frames without contrast medium; (2) a nonlinear histogram mapping is performed between the background image and all the frames in the sequence to remove the potential global brightness change throughout the sequence caused by automatic dose regulation in the X-ray imaging system; (3) a predefined aorta shape model is imposed via image-based semi-global 2-D/2-D registration to constrain the region for histogram calculation; (4) the dark trans-esophagus ultrasound (TEE) probe that potentially occludes part of the aorta is detected and excluded from histogram calculation; (5) the reference histograms with (without) contrast agent presence are formed from those frames with the largest (smallest) difference between the high percentile (e.g. 75) and low percentile (e.g. 5) of their image intensity distributions; (6) the contrast feature value for a frame is calculated as the ratio between its histogram similarity to the reference histogram with contrast agent and its histogram similarity to the reference histogram without contrast agent. Hence the contrast feature value is high for a frame containing contrast agent and low otherwise.

The method in [6,7] is very efficient and takes on average less than 1 s on a sequence consisting of ~150 frames. However, it is retrospective and requires the full acquisition of a whole X-ray sequence before contrast agent inflow detection can take place, meaning the detection is delayed. In order to minimize the delay, we propose an improved workflow for real-time contrast agent inflow detection. This real-time contrast agent inflow detection process is started and stopped automatically during TAVI procedures utilizing the X-ray acquisition signal, and the frames acquired between the two neighboring X-ray acquisition "start" and "stop" signals are treated as one image sequence. The key is to repetitively run the retrospective detection algorithm in [7] on all the frames acquired so far when a segment (e.g. 5) of new live X-ray frames are acquired, instead of waiting until the whole sequence is acquired, in order to achieve contrast agent inflow detection as fast as possible after the contrast agent is administered. The exact number of frames in each segment (i.e. the waiting interval) can be set by the user, depending on the preferred trade-off between the possible delay of contrast agent inflow detection and the overall processing efficiency.

During the process of repetitively calling the retrospective contrast agent inflow detection algorithm, as much as possible information is stored and then reused without recalculation to optimize the speed. For example, we can use the first 15 frames to calculate some indispensible information that will be used throughout the whole image sequence without recalculation, such as: (a) the reference image for histogram mapping, if needed, (b) background image for subtraction, and (c) the detected ultrasound probe mask. In addition, some relevant information for the frames already processed, such as their mapped images within the region of aorta (*ROA*), will be stored and then used without recalculation when new live frames come in. Furthermore, the case that there is no contrast agent presence for all the frames acquired so far is determined as early as possible, without having to go through all the steps in the contrast agent inflow detection algorithm. For example, when the frame index of the contrast template group drops when new live images come in, or when there is a high correlation between the contrast and background templates, it is determined as a non-contrast-enhanced case without further processing. Registration between the aorta shape model and the contrast template is the most time-consuming step. It is further skipped when the frame index for the contrast template group does not change much (i.e. less than 2) when new live images come in, and the previous registration results will be used.

When a potentially contrast-enhanced frame is detected, several steps need to be performed in order to confirm this frame as a contrast-enhanced frame. In particular, the first time a peak on the contrast feature curve is detected, the frame index for the peak is stored, and a notice about "a potential peak is detected" can also be sent to the user depending on user's setting. When a peak on the contrast feature curve is detected again with more live frames coming in, it will be compared with the previously stored peak and used to update the stored frame index for the peak if they are different. Otherwise if the newly detected peak is the same as the previously stored one, a final confirmation is needed after a few more frames are acquired. The final confirmation of contrast agent injection is based on the change of the contrast feature value for those frames immediately following the peak. This is because contrast medium tends to stay in the aortic root for a while before completely disappearing, thus the contrast feature value changes relatively slow after a correct (true) peak caused by contrast agent injection. In comparison, the contrast feature value tends to change very quickly after a false peak, for example, caused by body motion or respiration. Therefore false positives on the contrast agent injection detection due to body motion or respiration can be minimized by this final confirmation step.

3.2. 2-D X-ray image processing

Intra-operative X-ray images usually contain devices and/or structures that are not presented in the pre-operative 3-D volume, such as the catheter and TEE probe. In order to remove these irrelevant structures and enhance the aorta, a digitally subtracted image *SI* is calculated as:

$$SI = I - BI \tag{2}$$

where *I* is the 2-D aortic angiography that is detected in Section 3.1, and *BI* is the background image that could be obtained by enforcing a short period of image acquisition without contrast agent injection or by directly using the background image calculated in the contrast agent inflow detection algorithm. Due to cardiac and/or respiratory motion, there could be visible ghost artifacts in the digitally subtracted image *SI* (Fig. 7a). These ghost artifacts typically have high gradients and hence can negatively affect the accuracy

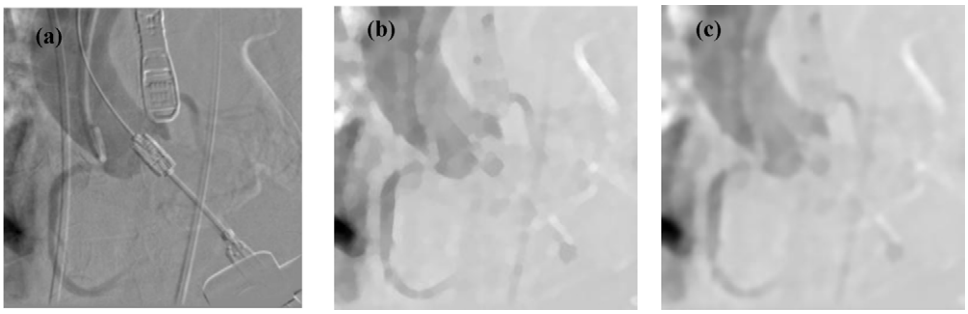

Fig. 7. 2-D X-ray image processing. (a) The digitally subtracted image (DSA) of an aortic angiography; (b) DSA image after morphological filtering; and (c) DSA image after Gaussian filtering.

of our registration algorithm, which utilizes a gradient-based similarity measure for registration (details are given in Section 3.4). In order to remove these ghost artifacts with high-gradients, we take advantage of the fact that the motion at the aorta between the background image and the aortic angiography is usually relatively small so that the ghost artifacts typically are spatially much smaller compared to the aorta. Hence we perform grayscale morphological closing and opening operations with an appropriate kernel size on the digitally subtracted image to remove small structures and keep the large one (i.e. the aorta):

$$MI = SI \bullet SE_1 \circ SE_2 \tag{3}$$

where '●' and '○' denote the morphological closing and opening operations, respectively. A closing operation eliminates small dark objects and an opening operation eliminates small bright objects. When they are performed sequentially, the ghost artifacts can be effectively reduced (Fig. 7b). SE_1 and SE_2 are the structure elements and are chosen to be disks with radius of 3 and 6 pixels (on a 256×256 image) respectively. Lastly, a Gaussian filter is applied on *MI* for smoothing in order to mitigate the artifacts produced by morphological filtering (Fig. 7c).

3.3. 3-D volume processing and DRR generation

The transformation relating points in the 3-D volume to points on the projected X-ray image consists of six extrinsic rigid-body parameters that are estimated by the iterative registration algorithm, and four intrinsic perspective projection parameters that are determined by the X-ray imaging system based on a pinhole camera model as depicted in Fig. 8. DRRs are generated using the 3-D texture-based volume rendering technique on the graphics processing unit (GPU), which yields better computational efficiency than software-based techniques such as ray-casting. It takes about 10 ms to generate 256×256 DRRs from a $256 \times 256 \times 256$ volume with an NVIDIA Quadro FX 580M.

DRR images rendered for the entire volume tend to be noisy, and some important landmarks such as the coronary ostia become faint or even invisible (Fig. 9a). To achieve robust and accurate registration, we utilize the segmentation of the aorta and the detected landmarks obtained by the method in [5] as mentioned earlier. An appropriate transparency is automatically selected to map the rendered DRR image to [0255], maximizing the dynamic range while eliminating saturation. The DRR image for the segmented aorta, denoted by I_A, is shown in Fig. 9b, with a significantly enhanced aorta compared to Fig. 9a. Note that the leaflets are not explicitly segmented, as evidenced by its mesh representation in Fig. 9c. However, the shape of the leaflets is clearly visible in the generated DRRs, demonstrating the advantage of our hybrid registration method using DRRs from the aorta segmentation mask VM_A, in comparison to conventional feature-based methods solely relying on the segmentation mask. Furthermore, explicit aorta segmentation on the 2-D image is not needed in our method. Instead the raw 2-D X-ray image, denoted by I_{DSA}, is used for registration purposes, after the image preprocessing steps as elaborated in Section 3.2. In comparison, conventional feature-based methods require segmentations of the corresponding structures on both the 3-D and 2-D data.

It is not straightforward to segment the coronary arteries from the 3-D volume directly due to their relatively high geometrical variations across patients. Instead, landmarks at the left and right coronary ostia are detected using the method in [5]. Conventional landmark-based registration algorithms require that the corresponding landmarks are also detected on the 2-D X-ray images, which is a challenging task and typically requires user interactions. Furthermore, it requires that the accuracy on the landmark position is relatively high on both the 3-D volume and 2-D images. In our hybrid method, we extend the detected landmarks to their surrounding area, in particular, the proximal part of the coronary artery, by optimizing the DRR generation of the small sphere around the detected ostia. The DRR image optimized for showing the coronary artery, without coronary artery segmentation from the 3-D volume, is then matched to the coronary artery shown in the X-ray image using intensity-based registration.

DRR images are generated from the two spherical masks, VM_C, around the left and right coronary ostia, which may have dark disk-like artifacts (Fig. 9d). We take advantage of the fact that the voxels

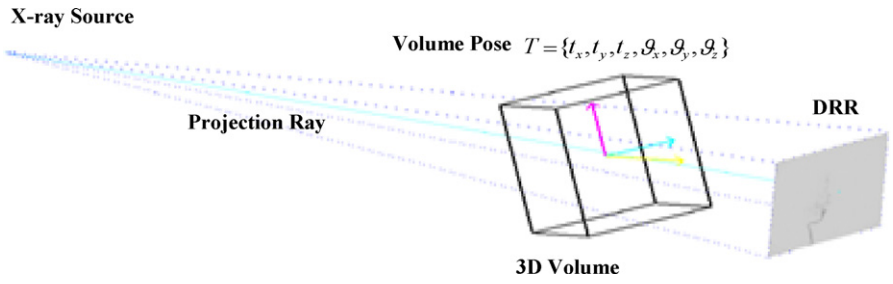

Fig. 8. Diagram for the generation of DRRs for 2-D/3-D registration.

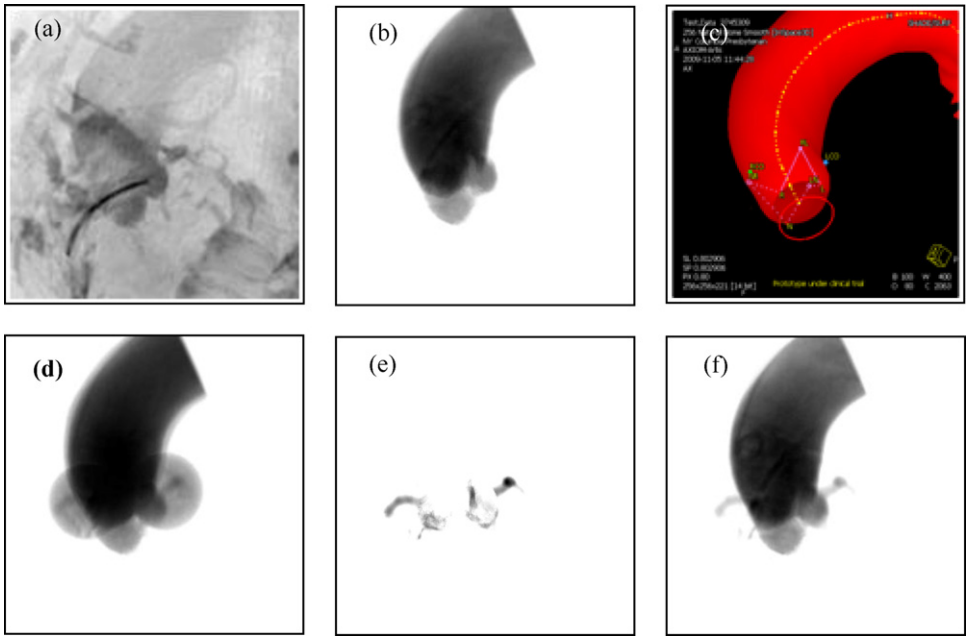

Fig. 9. 3-D volume processing and DRR generation. (a) DRR image generated from the original 3-D volume; (b) DRR image of the segmented aorta; (c) mesh model of the segmented aorta; (d) DRR image generated combining the aorta and coronary ostia, with the default rendering parameters; (e) DRR image of the coronary ostia artery with the automatically selected optimum rendering parameters; and (f) DRR image combining the aorta and the coronary ostia, with the automatically selected optimum rendering parameters.

in coronary arteries typically have a higher intensity than their surrounding structures due to the contrast agent, and their size relative to the spherical mask can be roughly estimated according to patients' anatomy. The 3-D volume transfer function for DRR generation is therefore automatically optimized in order to generate an optimal DRR image (denoted by I_c) showing the coronary artery only, as shown in Fig. 9e. In particular, a mask VM_{out} is obtained from the mask VM_C by excluding the area inside the aorta segmentation mask VM_A. The intensity histogram of the voxels in the mask VM_{out} is calculated and the lower bound of the window and level of the 3-D volume transfer function is chosen at the 90 percentile of the intensity histogram. The upper bound of the window level is chosen to be the highest voxel intensity of the complete volume VM. A combined DRR image generated using the automatically selected optimum rendering parameters for both the aorta and the coronary ostia is shown in Fig. 9f.

3.4. Hybrid 2-D/3-D registration

For the aorta, the calculation of the similarity measure is constrained to the region near the aorta boundary. Other areas are excluded for the calculation of the similarity for two reasons: (1) they are relatively homogenous in the DRR image and (2) the contrast medium filling within the aorta in the X-ray image could be different from that in the 3-D volume so that they are not reliable for similarity comparison. The masks are computed from the gradient of the DRR image convolved with a Gaussian kernel and are updated iteratively during the registration. An example on the masks used during registration is shown in Fig. 10. In our method, gradient correlation between images I_1 and I_2 with the image mask M is defined as:

$$GC(I_1, I_2, M) = NCC\left(\frac{\partial I_1}{\partial x}, \frac{\partial I_2}{\partial x}, M\right) + NCC\left(\frac{\partial I_1}{\partial y}, \frac{\partial I_2}{\partial y}, M\right) \quad (4)$$

$NCC(I_1, I_2, M)$ denotes the normalized cross correlation between images I_1 and I_2 within the mask M and is defined as:

$$NCC(I_1, I_2, M) = \frac{\sum_{M(x,y)=1}\left[I_1(x,y) - \bar{I}_1(x,y)\right]\left[I_2(x,y) - \bar{I}_2(x,y)\right]}{\sqrt{\sum_{M(x,y)=1}\left[I_1(x,y) - \bar{I}_1(x,y)\right]^2\left[I_2(x,y) - \bar{I}_2(x,y)\right]^2}} \quad (5)$$

where $\bar{I}$ is the average intensity of pixels in the mask M. The final similarity measure is defined as the summation of the gradient

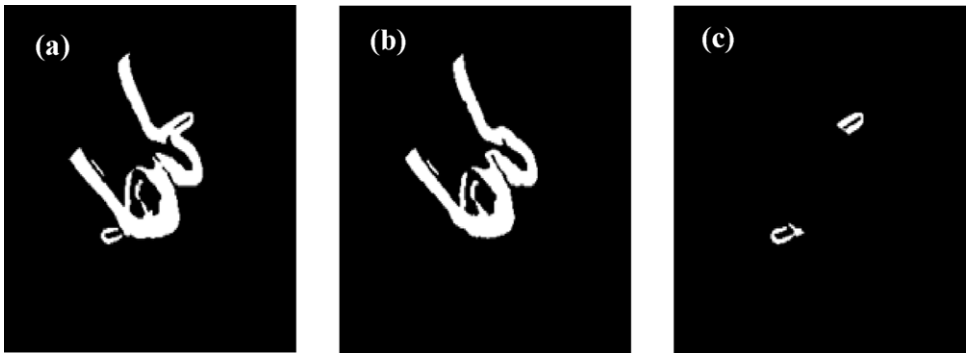

Fig. 10. Registration masks. (a) Mask including both the aorta and coronary arteries; (b) aorta mask M_A; and (c) coronary ostia mask M_C.

correlations in the aorta mask M_A and in the coronary ostia mask M_C:

$$SM = GC(I_A, I_{DSA}, M_A) + \beta \cdot GC(I_C, I_{DSA}, M_C) \quad (6)$$

where β controls the weight for the similarity of the coronary ostia landmark in the overall similarity calculation. Essentially the similarity measure combines the information from both the aorta and the extended coronary ostia landmarks. The information from the aorta provides a robust global alignment of the aorta, while landmarks provide additional information for a more accurate alignment at the structure of interest, as well as additional confirmation when there are multiple plausible candidate positions when using the aorta alone, which is possible when the contrast medium is relatively faint or partially washed out in the aorta.

The searching strategy for the six rigid-body parameters (3 translations and 3 rotations) in our hybrid registration method consists of three layers. At each layer, two DRR images, one for the aorta (I_A) and the other for the coronary artery landmark (I_C), are generated and compared simultaneously with the 2-D X-ray image (I_{DSA}) using the similarity measure defined in Eq. (6). In the coarse alignment layer, the DRR image of the aorta, I_A, is downsampled to 64×64. This low resolution is chosen for the improved efficiency and the smoothness of the similarity measure. Because the coronary mask focuses on small structures, a higher resolution of 128×128 is used for the DRR image of the coronary ostia/artery, I_C. The global search focuses on the estimation of in-plane translations with a few levels of fixed scaling (i.e. translation in the depth direction). Before starting the global search, the center of the aortic root is estimated through the positions of the two ostia landmarks and is moved to the center of the X-ray image. Then the similarity measure is computed in the range of $[-20\,\text{cm}, 20\,\text{cm}] \times [-20\,\text{cm}, 20\,\text{cm}]$. The global search is performed five times at $z_1 = [0.87, 0.93, 1.0, 1.07, 1.15]z_0$, where z_0 is the initial depth.

In the refinement layer, all images have the same resolution of 256×256, and four degrees of freedom (DOF) are searched, including 3-D translations and in-plane rotation. The optimization starts independently from the five registered positions provided by the coarse alignment layer. The first three registered positions with the largest similarity measures are selected as the starting position for the final layer, where a rigid-body transformation comprising three translations and three rotations is estimated. The one among the three registration results with the largest similarity measure is then selected as the final registration result.

4. Experiments and results

For automatic contrast-based 2-D/3-D registration, we offline tested the proposed algorithm on 34 patients with data acquired during TAVI procedures from 3 hospitals on a Siemens AXIOM Artis C-Arm system. For each patient, there is one 3-D C-Arm CT

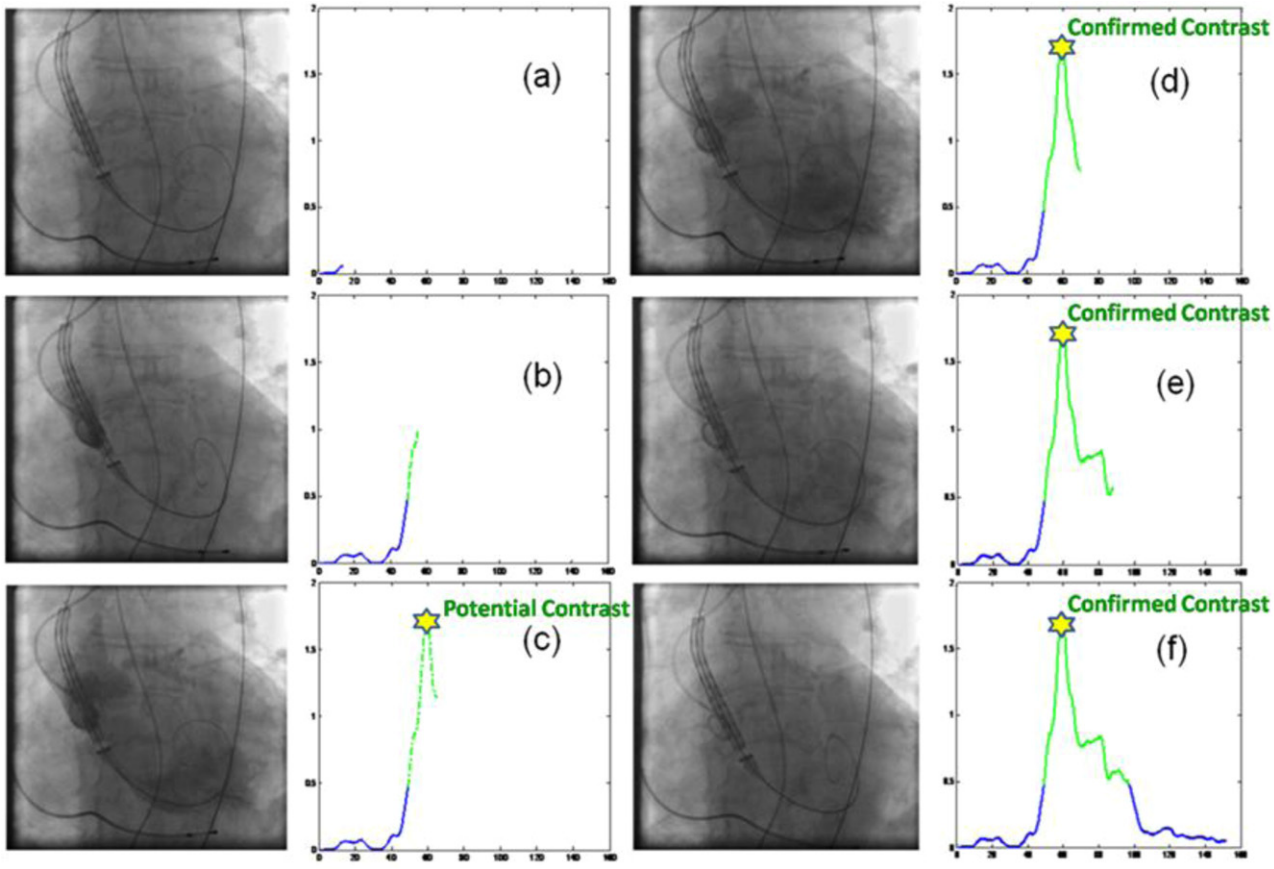

Fig. 11. Real-time contrast agent inflow detection. The left column shows the current frame, and the right column shows the contrast feature curve for all the frames processed so far. Blue on the contrast feature curve indicates no contrast agent with a low contrast feature value, while green indicates a potentially contrast-enhanced frame with a high contrast feature value. (a) There is no contrast medium, and the contrast feature curve is in blue. (b) Contrast medium start to appear, yet not to the peak, and the corresponding part of the contrast feature curve is shown in green dots. (c) The most contrast-enhanced frame is detected as a peak on the contrast feature curve. Optionally a notice can be sent to the user as "a potentially contrast-enhanced frame found". (d) The contrast-enhanced frame is confirmed when the newly detected contrast-enhanced frame is the same as the previously stored one and the contrast feature value stays high for a given number of frames. The contrast feature curve is now plotted in solid line. (e) The contrast feature value continues to drop when the contrast agent washes out from the aorta. (f) End of all the frames for this angiographic sequence, with those frames with a low contrast feature value again shown in blue on the contrast feature curve. (For interpretation of the references to color in this figure legend, the reader is referred to the web version of the article.)

volume of a typical size of $521 \times 512 \times 400$ and a resolution of 0.49 mm, one angiography of a typical size of 1024×1024 and a resolution of 0.154 mm, and may or may not have non-contrast-enhanced fluoroscopic sequences. In total there are 34 angiographic sequences showing the aortic root and 28 non-contrast-enhanced fluoroscopic sequences. Each sequence consists of 40–250 frames, and each frame is down-sampled to 256×256 for computational efficiency without a noticeable loss of accuracy on both contrast agent inflow detection and 2-D/3-D registration. All parameters in the contrast agent inflow detection and 2-D/3-D registration algorithms are set to the same values when experimenting on the patients' data. The algorithm is implemented in C++ and the computational time is reported on a single-core Dell PC that has an Intel Xeon processor at 1 GHz and 2 G memories, and a NVIDIA Quadro FX 580 graphics card.

For real-time contrast agent inflow detection, we simulate the scenario of live X-ray image acquisition and process the sequence in an increment of five frames. An example of real-time contrast agent inflow detection process is shown in Fig. 11. The average delay between the peak of the contrast feature curve (i.e. when the most contrast-enhanced frame is available) and the confirmation of contrast agent injection by our real-time algorithm is 10.9 frames, which is ~0.7 s for the X-ray acquisition speed of 15 frames/s typically used during TAVI procedures. In addition, the total time for processing a sequence of ~150 frames is on average <3 s for our real-time contrast agent inflow detection algorithm, which only triples the time used by the retrospective method in [7]. The retrospective method is more efficient because the detection needs to be done only once on all the frames in the sequence. However, this is at the cost of a significantly delayed detection, which is on average ~6 s (~5 s for image acquisition after the peak plus ~1 s on algorithm execution). Our real-time version therefore has a very good compromise between the overall efficiency and the fast response, which is achieved through the optimized process and workflow that minimizes redundant calculations, as elaborated in Section 3.1.

All the tested sequences are correctly classified as with or without contrast agent injection in our experiments. For the contrast-enhanced sequences, the detected frame is further compared to the manual annotation of the start and stop of the contrast agent presence in the aortic root. All the frames within the range of manual annotation are highly correlated in appearance and contain sufficient contrast medium, and hence are assumed to be non-differentiable for detection and registration purposes. For all the contrast-enhanced sequences, the detected frame is confirmed to be within the manually annotated contrast range, and is then used for the subsequent 2-D/3-D registration.

To evaluate the 2-D/3-D registration accuracy, we use two coronary ostia and two hinge points (the lowest points of the aortic leaflets) that are automatically detected on 3-D volumes (Fig. 12). After registration, the 2-D projections of these landmarks are compared with the corresponding 2-D projections using the optimal registration pose (the ground truth pose), which are manually selected by an expert under a physician's supervision. Because the accuracy of the registered coronary ostia and the hinge plane are both very important from a clinical perspective for TAVI procedures, they are evaluated separately in our experiment. The accuracy of coronary ostia overlay is evaluated by the average 2-D distance of the projected coronary ostia between our 2-D/3-D registration results and the ground truth pose. The accuracy of the hinge plane position is measured by the 2-D distance of the hinge line connecting the two hinge points. While rigid-body registration is needed in order to handle out-of-plane rotation, performance evaluation on a 2-D plane is appropriate for TAVI procedures, because the C-Arm angulation does not change after the optimal angle is selected, and the most important guidance are the landmarks (i.e. the ostia and hinge points) on the optimal image plane.

The error is first computed for the calibration-based method, which overlays the 3-D model onto the fluoroscopy using the machine parameters, including the C-Arm primary and secondary angles, the source to object distance, the source to detector distance, and the pixel spacing. This is the accuracy that can be achieved relying solely on machine calibration without patient-specific 2-D/3-D registration. It is observed that on average the ostia distance for 34 cases is 15.35 mm and the hinge plane distance is 14.21 mm. These large errors demonstrate that significant patient movements and aortic root movements do exist during TAVI interventions. Hence 2-D/3-D registration is a necessary step to compensate for the movement for an accurate 2-D/3-D fusion.

Furthermore, the proposed method is compared with the conventional intensity-based 2-D/3-D registration method. In the conventional method, the original angiographic image and 3-D volume are used without preprocessing, and the DRR image is generated from the whole 3-D volume without segmentation [24]. We apply the same hierarchical registration strategy and the same similarity measure (i.e. gradient correlation) for a fair comparison. Quantitative experimental results on 34 cases are summarized in Table A1 (Appendix A). For a qualitative inspection, examples of registration results with different magnitudes of errors are shown in Figs. 12 and 13.

From Table A1, we can see that the proposed method achieves sub-millimeter (0.66 mm) accuracy on average, which significantly outperforms the conventional method (15.11 mm). Clinically, a distance error of <1.5 mm is considered to be good (97% in our

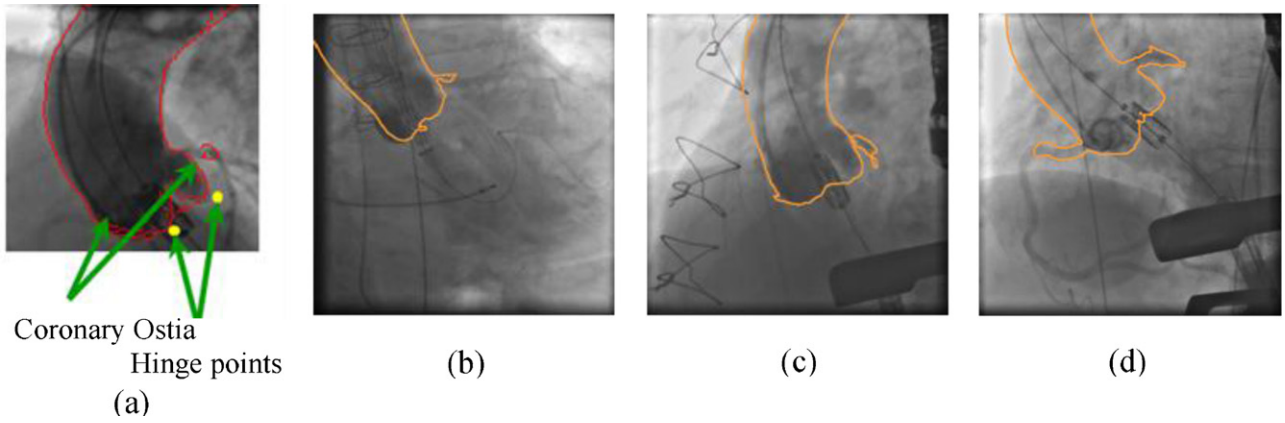

Fig. 12. (a) A schematic view of evaluation of registration accuracy; (b) an example of registration error of ~2 mm (5 pixels); (c) an example of registration error of ~1 mm and (d) an example of registration error of <0.5 mm.

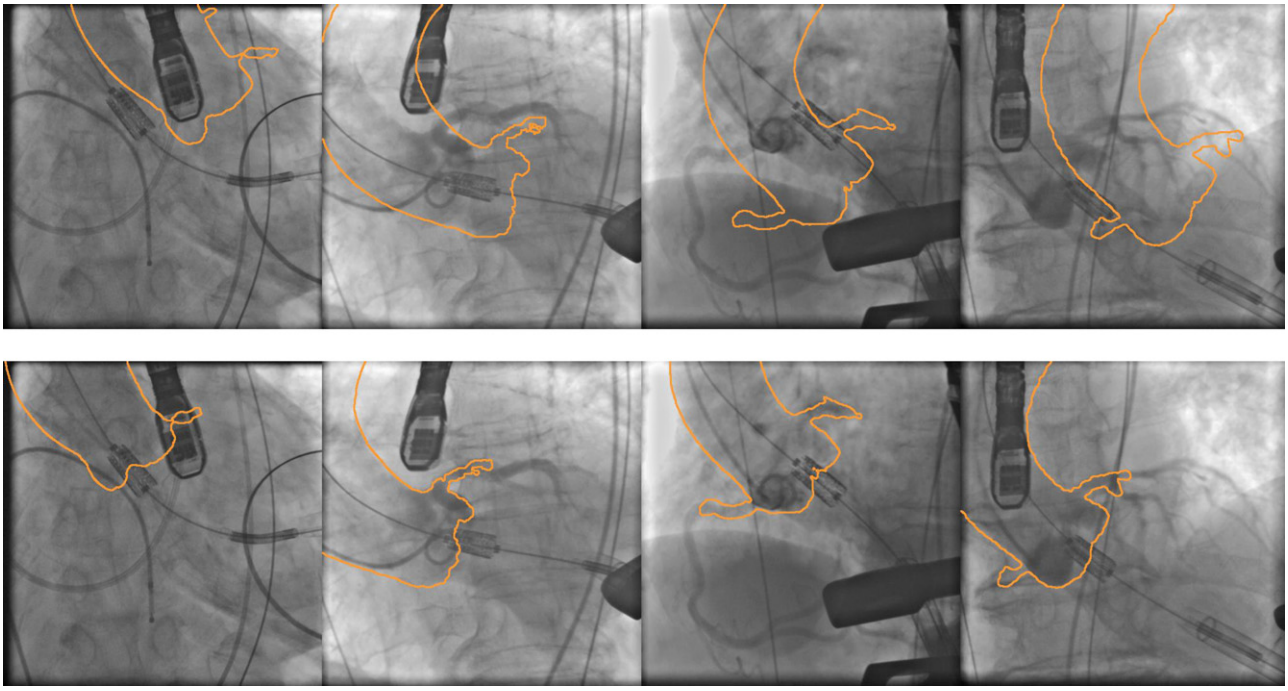

Fig. 13. Examples of registration results by overlaying the edge map of the DRR image onto the angiography. The upper row shows the initial position, and the lower row shows the overlay after our hybrid-2-D/3-D registration.

experiments), 1.5–3 mm to be acceptable (3%), and >3 mm to be inappropriate (0%). In addition, the initial error before registration (by auto-centering the volume) is as large as 52.92 mm, demonstrating the extremely high robustness and large capture range of the proposed method. The conventional method largely failed for some cases due to the trap into a local minimum. As shown in Fig. 9a, the DRR image generated from the 3-D volume without segmentation and preprocessing includes many irrelevant structures and has a very low signal-to-noise ratio. These irrelevant structures make the similarity measure profile highly non-convex and dramatically increase the chance of the optimizer being trapped into a local minimum. In addition, for successful cases, the proposed hybrid method outperforms the conventional method is terms of accuracy at the landmark of interest, i.e. the coronary ostia in our case, by integrating the landmark information into the intensity-based registration.

The angle between the normal vector of the hinge plane determined by the three hinge points after registration and that from annotations is also calculated, and is found to be as small as 1.38° on average for the proposed method. This is an important measurement because it is critical for the implanted prosthesis to be coaxial to the patients' natural valve. Clinically, a tilting <5° can be stated as good (94% in our experiments), 5–10° as acceptable (6%), and >10° as inappropriate (0%). These values show that our method has the great potential to meet the clinical needs in terms of accuracy. In comparison, the conventional method results in a tilting error >10° for as many as 9 cases (27%).

5. Discussion and conclusion

We presented a novel contrast-based 2-D/3-D registration method for motion compensation in our image guidance system for TAVI. To the authors' best knowledge, this is the first fully automatic 2-D/3-D fusion system designed for image guidance using interventional C-Arm CT during TAVI procedures. TAVI is one of the most important applications in the hybrid operating room that all the major imaging companies are advancing toward and/or working on, especially after the recent FDA approval of the Edwards SAPIEN aortic valve. The procedure is relatively complicated and requires highly accurate image guidance for proper positioning and deployment of the prosthetic valve in the millimeter range. The information provided by our image guidance system is essential to ensure that the device covers the old valve without permitting leakage and that it does not cover the coronary ostia – the end points of the coronary arteries – which would cause an immediate heart attack.

A seamless workflow is an indispensable pre-requisite for an image guidance system to be well utilized during TAVI that involves complicated operations and a large multi-disciplinary team. Our system is specifically designed for TAVI by ensuring full automation and a low computational cost. Each step in the proposed algorithm is optimized in efficiency and fully automatic, including contrast agent inflow detection, its extension to a real-time version, optimized DRR generation for 2-D/3-D registration, and optimized volume visualization. In comparison, for many other image guidance systems applied for other interventional applications, such as those reported in [25–27], motion compensation typically involves significant user interactions, including manual selection of the best angiographic frame for registration, user adjustment of the parameters for DRR generation for 2-D/3-D registration, as well as interactive editing of the window-level settings for volume visualization.

The contrast agent inflow detection algorithm is based on histogram analysis and a likelihood ratio test, making it highly robust to variations across different patients and imaging protocols. The real-time version maintains a high detection accuracy similar to that achieved by the retrospective method in [7], while providing a fast response to the event of contrast medium injection so that 2-D/3-D registration can be performed as soon as possible. Segmentation and landmark information on the 3-D volume are furthermore integrated with image intensity information to accurately re-align the 3-D model to the patient. This hybrid method does not require explicit aorta segmentation and landmark detection on the 2-D X-ray image, which is by itself a very difficult

Table A1
Validation of the proposed 2-D/3-D registration method in comparison with the conventional method on clinical data.

#	Ostia distance (mm)			Hinge plane distance (mm)			Average distance (mm)			Hinge plane angle (degree)		
	Init.	Conv.	Prop.	Init.	Conv.	Prop.	Init.	Conv.	Prop.	Init.	Conv.	Prop.
1	50.65	12.33	0.23	25.04	43.46	0.37	37.85	27.90	0.30	9.61	17.62	1.69
2	48.42	8.49	0.06	33.50	14.31	0.40	40.96	11.40	0.23	8.74	6.77	0.37
3	31.86	66.29	0.06	23.01	70.28	0.11	27.44	68.29	0.09	7.17	12.36	0.49
4	29.05	0.60	0.01	19.54	0.97	0.10	24.29	0.79	0.06	3.23	9.03	0.06
5	25.19	0.30	0.20	25.13	1.00	0.27	25.16	0.65	0.24	5.80	3.93	2.95
6	51.70	25.50	0.02	27.04	46.81	0.25	39.37	36.16	0.14	5.61	1.41	0.06
7	22.24	0.37	0.92	17.12	1.25	0.85	19.68	0.81	0.89	3.95	0.89	5.78
8	53.07	0.46	0.01	64.77	1.47	0.02	58.92	0.97	0.02	1.53	4.04	0.06
9	15.53	0.12	0.70	28.31	0.71	0.74	21.92	0.42	0.72	9.18	2.38	1.05
10	67.05	4.21	0.66	90.55	4.64	1.14	78.80	4.43	0.90	1.87	1.93	0.07
11	37.25	0.58	0.48	28.46	2.96	0.89	32.85	1.77	0.69	5.78	7.97	2.00
12	147.87	0.80	0.41	189.62	3.18	0.64	168.75	1.99	0.53	2.41	9.80	0.44
13	42.07	1.66	1.00	42.93	1.27	1.34	42.50	1.47	1.17	9.77	6.68	0.16
14	32.36	0.96	0.90	61.36	2.17	1.44	46.86	1.57	1.17	8.77	6.50	2.34
15	49.64	1.98	1.14	57.89	2.50	0.84	53.77	2.24	0.99	7.19	5.04	2.73
16	90.04	1.70	0.41	48.10	1.82	0.82	69.07	1.76	0.62	0.72	10.81	0.58
17	72.25	0.33	0.60	67.46	1.61	1.62	69.86	0.97	1.11	0.93	2.46	7.31
18	34.32	21.01	0.10	11.12	23.79	0.65	22.72	22.40	0.38	6.18	15.92	1.91
19	140.12	0.24	0.19	172.60	1.03	0.50	156.36	0.64	0.35	2.78	5.67	2.60
20	34.68	46.97	1.21	21.59	54.52	1.58	28.14	50.75	1.40	4.39	12.82	0.91
21	24.95	10.33	0.29	67.51	50.46	0.77	46.23	30.40	0.53	6.56	12.53	0.38
22	132.63	42.34	0.74	153.12	47.38	1.59	142.88	44.86	1.17	1.12	6.15	3.63
23	32.90	46.91	1.40	22.77	47.97	1.85	27.83	47.44	1.63	5.73	4.34	2.79
24	17.03	37.69	0.65	49.52	39.37	2.16	33.27	38.53	1.41	1.32	1.79	1.08
25	50.99	3.92	0.39	24.49	6.19	0.85	37.74	5.06	0.62	6.55	3.58	0.80
26	33.79	4.24	0.02	32.82	24.27	0.16	33.30	14.26	0.09	4.25	15.75	0.32
27	48.51	1.13	0.83	17.65	4.22	0.66	33.08	2.68	0.75	2.27	6.34	1.43
28	64.82	2.78	0.00	58.70	3.79	0.03	61.76	3.29	0.02	9.35	2.56	0.00
29	19.98	17.23	0.57	48.54	27.68	2.20	34.26	22.46	1.39	3.48	6.72	0.06
30	42.49	0.24	0.27	20.49	1.40	1.37	31.49	0.82	0.82	1.52	2.78	4.30
31	106.72	0.34	0.16	167.20	2.06	0.16	136.96	1.20	0.16	2.14	7.24	0.57
32	37.92	0.48	1.14	48.74	3.03	1.36	43.33	1.76	1.25	4.09	13.92	0.06
33	46.20	35.78	0.59	56.30	9.95	0.41	51.25	22.87	0.50	1.82	7.32	0.74
34	17.77	50.39	0.32	23.12	31.31	0.37	20.45	40.85	0.35	3.56	10.73	0.57
Average	51.53 ± 33.90	13.20 ± 18.83	0.49 ± 0.40	54.30 ± 47.18	17.02 ± 20.70	0.84 ± 0.61	52.92 ± 39.53	15.11 ± 18.95	0.66 ± 0.47	4.69 ± 2.85	7.23 ± 4.59	1.48 ± 1.73

problem due to the low image quality and information loss resulting from perspective projection. Our experiments on clinical data from 34 patients show that compared to the conventional intensity-based 2-D/3-D registration method, the proposed method reduces the average error from 15.11 mm to 0.66 mm.

Our contrast-based motion compensation can be achieved within 2.5 s (1 s for contrast agent inflow detection and 1.5 s for 2-D/3-D registration) after the most contrast-enhanced frame is available. It has been confirmed with our clinical collaborating doctors that a fast response for efficient motion compensation is important during TAVI procedures due to its high complexity and the stringent requirement on the registration accuracy so that decision-making is time-sensitive. Integration of the proposed contrast-based 2-D/3-D registration algorithm into our 2-D/3-D fusion system is under way, and clinical trials on a large number of patient data during live cases are planned for the near future.

Other future work includes dynamic weight determination for intensity and landmark features and live motion compensation. Currently rapid pacing is used during valve deployment to minimize cardiac and/or respiratory motion. Experienced doctors could also mentally compensate for cardiac/respiratory motion by prediction (due to its pseudo-periodic nature) in practice. It requires further clinical experiments to better understand the impact of uncompensated cardiac/respiratory motion for TAVI procedures. In particular, image-based automatic motion-phase detection [28] and contrast range detection [29] can be utilized to fully explore the pseudo-cyclic property of the aortic motion, and hence static 2-D/3-D registration can be extended to register the 3-D model to a sequence of angiographic images.

Acknowledgements

The authors are thankful to Dr. Matthias John and Mr. Alois Nöttling from Siemens AX Germany for providing the data in this study.

Appendix A.

Table A1.

References

[1] Nkomo VT, Gardin JM, Skelton TN, Gottdiener JS, Scott CG, Enriquez-Sarano M. Burden of valvular heart diseases: a population-based study. Lancet 2006;368(10):1005–11.
[2] Durand E, et al. Transfemoral aortic valve replacement with the Edwards SAPIEN and Edwards SAPIEN XT prosthesis using exclusively local anesthesia and fluoroscopic guidance. JACC Cardiovasc Intervent 2012;5(5):461–7.
[3] Smith CR, Leon MB, Mack MJ, et al. Transcatheter versus surgical aortic-valve replacement in high-risk patients. New Engl J Med 2011;364(23): 2187–98.
[4] John M, Liao R, Zheng Y, Nottling A, Boese J, Kirschstein U, et al. System to guide transcatheter aortic valve implantations based on interventional C-Arm CT imaging. LNCS 2010;6361:375–82. MICCAI 2010.
[5] Zheng Y, John M, Liao R, Boese J, Kirschstein U, Comaniciu D. Automatic aorta segmentation and valve landmark detection in C-Arm CT: application to aortic valve implantation. LNCS 2010;6361:476–83. MICCAI 2010.
[6] Liao R, You W, Yan M, John M. Automatic detection of contrast injection on fluoroscopy and angiography for image guided trans-catheter aortic valve implantations (TAVI). Proc SPIE 2011;7964. pp. 79640Z–79640Z-7, SPIE 2011.
[7] Liu Y, Liao R, Lv X. Extended contrast detection on fluoroscopy and angiography for image guided trans-catheter aortic valve implantations (TAVI). Proc SPIE 2012;8316. pp. 831618–1831618-9, SPIE 2012.

[8] Miao S, Liao R, Zheng Y. A hybrid method for 2-D/3-D registration between 3-D volume and 2-D angiography for trans-catheter aortic valve implantation (TAVI). Proc IEEE ISBI 2011:1215–8. ISBI 2011.
[9] Liu A, Bulliitt E, Pizer SM. 3D/2D registration via skeletal near projective invariance in tubular objects. LNCS 1998;1496:780–7. MICCAI 1998.
[10] Duong L, Liao R, Sundar H, Tailhades B, Meyer A, Xu C. Curve-based registration of coronary vessels for image guided navigation in interventional cardiology. Proc SPIE 2009;7261. pp. 72610S–172610S-10, SPIE 2009.
[11] Kita Y, Wilson DL, Nobel JA. Real-time registration of 3D cerebral vessels to X-ray angiograms. LNCS 1998;1496:1125–33. MICCAI 1998.
[12] Hipwell JH, Penney GP, McLaughlin RA, Rhode KS, Summers PE, Cox TCS, et al. Intensity-based 2D3D registration of cerebral angiograms. IEEE Trans Med Imaging 2003;22(11):1417–26.
[13] Penney GP, Weese J, Little JA, Desmedt P, Hill DLG, Hawkes DJ. A comparison of similarity measures for use in 2D3D medical image registration. IEEE Trans Med Imaging 1998;17(4):586–95.
[14] Lemieux L, Jagoe R, Fish DR, Kitchen ND, Thomas DG. A patient-to-computed-tomography image registration method based on digitally reconstructed radiographs. Med Phys 1994;21(11):1749–60.
[15] Gessat M, Merk DR, Falk V, Walther T, Jacobs S, Nöttling A, et al. A planning system for transapical aortic valve implantation. Proc SPIE 2009;7261. pp. 72611E–72611E-12, SPIE 2009.
[16] Ionasec R, Georgescu B, Gassner E, Vogt S, Kutter O, Scheuering M, et al. Dynamic model-driven quantification and visual evaluation of the aortic valve from 4D CT. LNCS 2008;5241:686–94. MICCAI 2008.
[17] Karar ME, Chalopin C, Merk DR, Jacobs S, Walther T, Falk V, et al. Localization and tracking of aortic valve prosthesis in 2D fluoroscopic image sequences. Proc SPIE 2009;7261. pp. 72611Q–72611Q-8, SPIE 2009.
[18] Li M, Mazilu D, Horvath KA. Robotic system for transapical aortic valve replacement with MRI guidance. LNCS 2008;5241:476–84. MICCAI 2008.
[19] Lang P, Seslija P, Chu MWA, Bainbridge D, Guiraudon GM, Jones DL, et al. US–fluoroscopy registration for transcatheter aortic valve implantation. IEEE Trans Biomed Eng 2012;59(5):1444–53.
[20] Kempfert J, Falk V, Schuler G, Linke A, Merk DR, Mohr FW, et al. DynaCT during minimally invasive off-pump transapical aortic valve implantation. Ann Thorac Surg 2009;88(6):2041.
[21] Zellerhoff M, Scholz B, Ruehrnschopf EP, Brunner T. Low contrast 3D reconstruction from C-arm data. Proc SPIE 2005;5745:646–55. SPIE 2005.
[22] Condurache A, Aach T, Eck K, Bredno J. Fast detection and processing of arbitrary contrast agent injections in coronary angiography and fluoroscopy. Proc CEUR 2004;116:5–9. CEUR 2004.
[23] Chen T, Funka-Lea G, Comaniciu D. Robust and fast contrast agent inflow detection for 2D X-ray fluoroscopy. LNCS 2011;6891:243–50. MICCAI 2011.
[24] Khamene A, Bloch P, Wein W, Svatos M, Sauer F. Automatic registration of portal images and volumetric CT for patient positioning in radiation therapy. Med Image Anal 2005;10(1):96–112.
[25] Fu D, Kuduvalli G. A fast, accurate, and automatic 2D–3D image registration for image-guided cranial radiosurgery. Med Phys 2008;35(5):2180–94.
[26] Groher M, Zikic D, Navab N. Deformable 2D–3D registration of vascular structures in a one view scenario. IEEE Trans Med Imaging 2009;28(6):847–60.
[27] Liao R. 2-D/3-D registration of computed tomographic volumes with fluoroscopic images by spines for EP applications. Proc IEEE ISBI 2010:1213–6. ISBI 2010.
[28] Sundar H, Khamene A, Yatziv L, Xu C. Automatic image-based cardiac and respiratory cycle synchronization and gating of image sequences. LNCS 2009;5762:381–8. MICCAI 2009.
[29] You W, Liao R, Yan M, John M. Spatial–temporal analysis for automatic contrast injection detection on angiography during trans-catheter aortic valve implantations. Proc IEEE ISBI 2010:702–6. ISBI 2010.